Remote Sensing for Earth Observation and Surveillance
Assignment #1

Fontan Anna, 945648

1 Notation

Table 1: Nomenclature of problem 1

Name	Units	Nomenclature
B	[Hz]	Bandwidth
K	[$\frac{m^2 kg}{s^2 K}$]	Boltzmann constant
T	[K]	Brightness temperature
ψ	[deg]	Direction of arrival of the signal
f_0	[Hz]	Frequency of the spectrum
f	[Hz]	Frequencies vector
N_f	[-]	Number of frequency samples
N_t	[-]	Number of time samples
T_{obs}	[s]	Observation time
$\Delta\varphi$	[deg]	Phase difference
P	[W]	Power
T_s	[s]	Sampling time
c	[$\frac{m}{s}$]	Speed of light
σ	[*]	Standard deviation
Δf	[Hz]	Step size of the frequency vector
V	[*]	Variance
λ	[m]	Wave length

where * stands for those values which units depend on the quantity considered to evaluate them.

Table 2: Nomenclature of problem 2

Name	Units	Nomenclature
v	[$\frac{mm}{day}$]	Displacement rate
k_z	[-]	Height-to-phase conversion factor
N_x, N_y	[-]	Number of samples for x and y
φ	[°]	Phase of the interferometer
z	[m]	Surface topography
k_v	[-]	Velocity-to-phase conversion factor

Table 3: Symbols

Name	Nomenclature
A	Amplitude
R	Auto-correlation
C	Covariance matrix
H	Filter (frequency domain)
$\mathbf{d}_1$	First column of **d**, signal received by antenna 1
D_1	Fourier Transform of $\mathbf{d}_1$
D_2	Fourier Transform of $\mathbf{d}_2$
d	Matrix of the signals
S	Power spectrum of the signal
$\mathbf{d}_2$	Second column of **d**, signal received by antenna 2
A, B, C	Three emitting sources

2 Problem 1: a passive Radiometer

2.1 Estimate the equivalent brightness temperature and assess the theoretical accuracy of it

In order to conduct a first and rough analysis of the signals emitted by the N sources, for each antenna the whole received spectrum here is assumed as radiated by just a single source. Moreover, the power spectrum of it is hypothesised constant over the whole available 10 MHz bandwidth.

Thus, since here only one source and two antennas are considered, the two resulting signals have been studied in the same way but separately and they are respectively given by the two column vectors of the matrix **d**. The following procedure is focused on the analysis of the signal received by the antenna that corresponds to the first column of **d** (d_1), but as stated the same method has been applied to the other too.

Since the power spectrum is assumed constant (hence it is flat in all the bandwidth), the received signal is a white process, hence unbiased; moreover, the power (P_{d_1}) is equal to the estimated one and it can be evaluated then as shown in Eq. 1.

$$\begin{cases} P_{d_1} = E[\mid d_1 \mid^2] = \dfrac{1}{N_t} \displaystyle\sum_{i=1}^{N_t} \mid d_1 \mid^2 & (1) \\ P_{d_1} = K B_{d_1} T_{d_1} & (2) \end{cases}$$

where the transmitted number of time samples is tabulated in Tab. 5.
Since the signal is assumed Circular Normal the following equations hold:

$$\begin{cases} E[d_1] = 0 & (3) \\ E[\mid d_1 \mid^2] = P_{d_1} = {\sigma_{d_1}}^2 & (4) \\ V(\mid d_1 \mid^2) = {\sigma_{d_1}}^4 = {P_{d_1}}^2 & (5) \\ V(P_{est,d_1}) = \dfrac{{P_{est,d_1}}^2}{BT_{obs}} & (6) \end{cases}$$

Thus, knowing the power of the source (shown in Tab. 4) through Eq. 1, the brightness temperature can be evaluated with Eq. 2.

Table 4: Powers and brightness temperatures

Name	Value	Name	Value
P_{d_1}	$9.643867 \cdot 10^{-16}$ W	P_{d_2}	$9.643889 \cdot 10^{-16}$ W
T_{d_1}	6.985 K	T_{d_2}	6.985 K

Table 5: Values of the problem

Name	Value
N_t	100000
T_s	10^{-7} s
T_{obs}	0.01 s

The accuracy of the estimation is given by the standard deviation of the power (which due to the assumptions is given by Eq. 7), since it is a measure of the dispersion of a set of values around their mean one.

$$\begin{cases} \sigma_{d_1}^2 = \sqrt{V(P_{est,d_1})} = \dfrac{P_{d_1}^2}{BT_{obs}} & (7) \\ \sigma_{T_1} = \dfrac{\sigma_{d_1}}{BK} & (8) \end{cases}$$

where the observation time is reported in Tab. 5.
The results are shown in Tab. 6: As reported in the table above, the results are the same for

Table 6: Standard deviations of the temperatures

Name	Value
σ_{T,d_1}	0.0221 K
σ_{T,d_2}	0.0221 K

the two antennas, as expected since they are considering the same (and unique) source.

2.2 Estimate the power spectrum of the signal at one of the antennas. How many distinct sources can you detect?

In order to estimate the power spectrum of antenna **1** (Eq. 9), the received signal has to be analysed in the frequency domain; hence, its Fourier Transform has been used, where the number of points in the frequency domain N_f is reported in Tab. 7.

$$S_{d_1} = \frac{1}{T_{obs}} D_1 D_1^* \tag{9}$$

The graph of the power spectrum of the signal received by the antenna **1** is shown in Fig. 1a,

Table 7: Number of samples

Name	Value
N_f	131072

while the auto-correlation is shown in Fig. 1b.

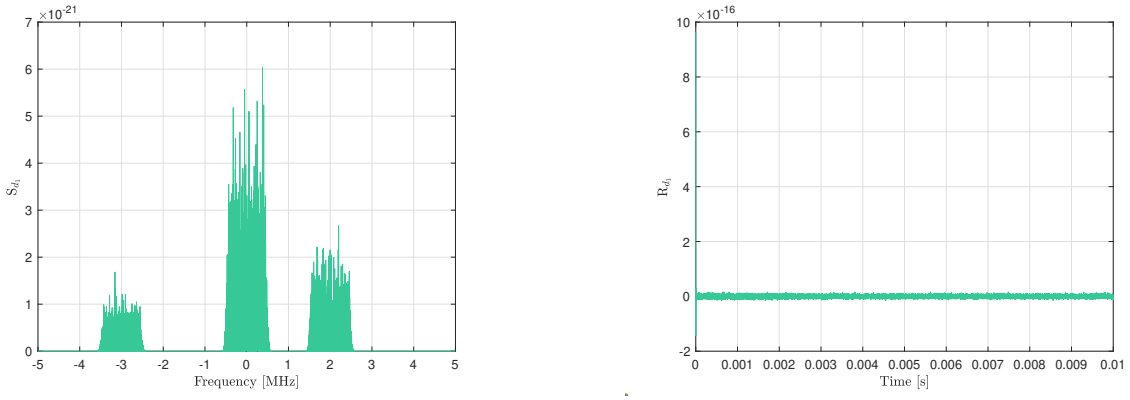

(a) S_{d_1} **(b)** R_{d_1}

Figure 1: Power spectrum and auto-correlation of d_1

In order to understand if the assumption of section 2.1 holds (i.e. of white process), the power spectrum of the signal has been plotted; in S_{d_1} one can notice three main peaks, affected by some errors, that represent the distinct sources that can be detected.
If the original signal is considered as in section 2.1 a white process, then its power spectrum should be constant in all the bandwidth. Since this is not happening with the signal, the assumption is wrong.
However, the auto-correlation has been evaluated too, through the Inverse Fourier Transform of the power spectrum S_{d_1} and then by scaling it as shown in Eq. 10:

$$R_{d_1} = \mathcal{F}^{-1}(S_{d_1})\Delta f N_f \tag{10}$$

where Δf is the step size of the frequencies vector.
If a signal is white then the plot of the auto-correlation has a nonzero value only in t = 0. This is the case of these signals, even if they are not white; however, similar results may be achieved.

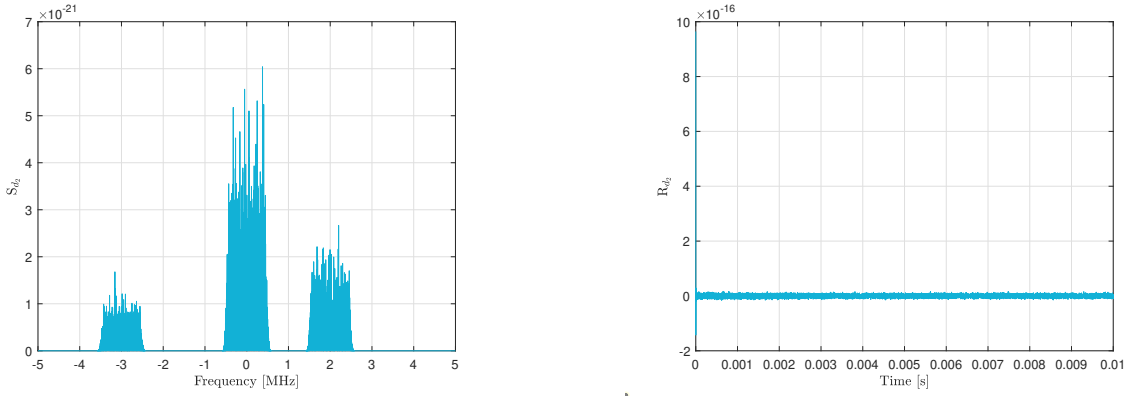

(a) S_{d_2} **(b)** R_{d_2}

Figure 2: Power spectrum and auto-correlation of d_2

2.3 Quantify bandwidth and frequency-shift of each detected source

As already stated in section 2.2, each antenna receives the radiation of three signals (Fig. 4a and Fig. 4b). Here the MATLAB function OBW has been exploited in order to evaluate the different bandwidths, through the selection of the proper frequency window for each case.

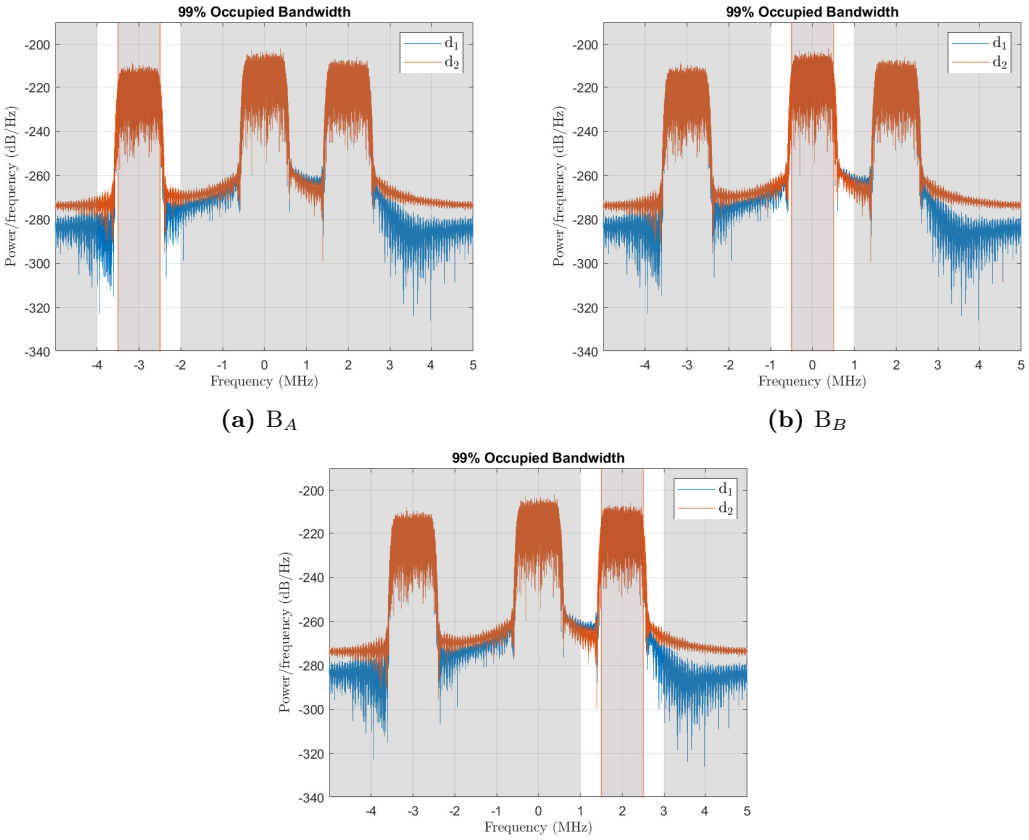

(a) B_A **(b)** B_B

(c) B_C

Figure 3: Evaluation of the bandwidths of the signals

As shown in Fig. 3a, Fig. 3b and Fig. 3c, six different values have been obtained for the bandwidths, that are:

Table 8: Bandwidths of the different sources

Source	B_{D_1}	B_{D_2}
A	1.00465 MHz	1.00466 MHz
B	1.00161 MHz	1.00162 MHz
C	1.00496 MHz	1.00498 MHz

while the frequency shifts and amplitudes (evaluated as the maximum value of each peak of the spectra in the frequency domain) are:

Table 9: Frequency shifts and amplitudes

Source	f_0	A_{D_1}	A_{D_2}
A	- 3 MHz	$4.1004 \cdot 10^{-12}$	$4.0975 \cdot 10^{-12}$
B	0 MHz	$7.7733 \cdot 10^{-12}$	$7.7724 \cdot 10^{-12}$
C	2 MHz	$5.1660 \cdot 10^{-12}$	$5.1647 \cdot 10^{-12}$

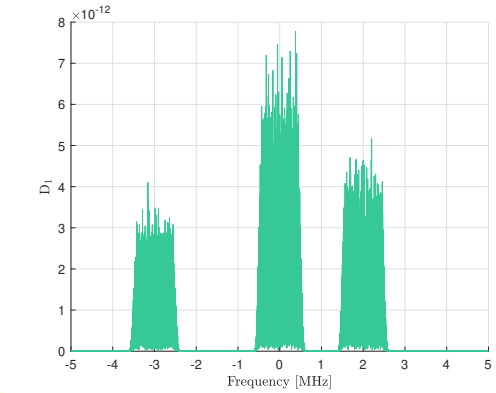

(a) D_1

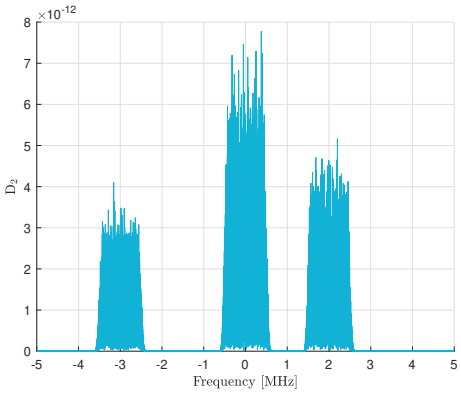

(b) D_2

Figure 4: Signals received by the antennas

2.4 Propose and implement an algorithm for the extraction of the signal associated with each detected source, and validate it by estimating its power spectrum

In order to extract the signals associated with the sources, three different filters have to be exploited for each antenna. Indeed, these filters are used to analyse the radiation of every single source while suppressing the other aspects of the entire signals.
In particular, the filters are built as rectangular pulses in the frequency domain (see Eq. 11), using as bandwidths and frequency shifts the data reported in Tab. 8 and in Tab. 9.

$$H_{d_i} = \mathcal{A}_{i,j}\text{RECT}\left(\frac{f - f_{i,j}}{B_j}\right) \tag{11}$$

where i = 1, 2 are the antennas and j = 1 (A), 2 (B), 3 (C) the three sources.
Thus, the results of the products between the signals in the frequency domain (Fig. 4a and Fig. 4b) and each filter (Fig. 5 and Fig. 6) are the six isolated peaks. Once the signals are filtered,

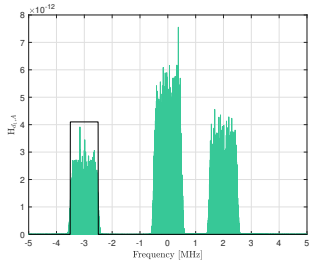

(a) $H_{1,A}$

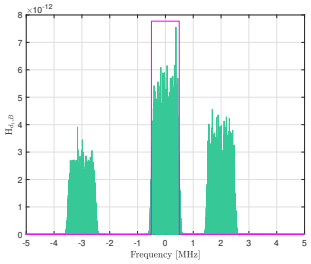

(b) $H_{1,B}$

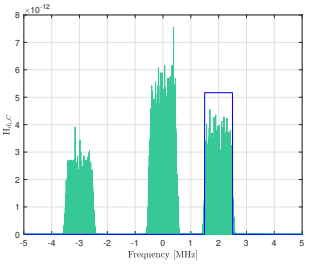

(c) $H_{1,C}$

Figure 5: Filters antenna **1**

their power spectra can be retrieved as already did in section 2.2 with Eq. 9; the results are shown in Fig. 7 and Fig. 8.

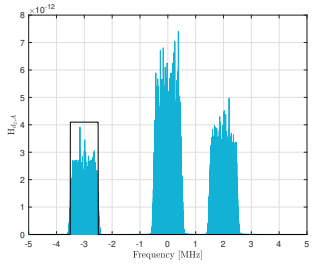

(a) $H_{2,A}$

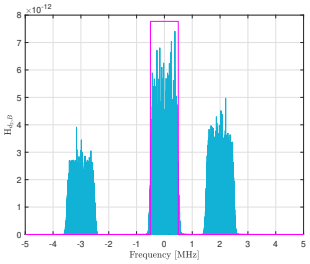

(b) $H_{2,B}$

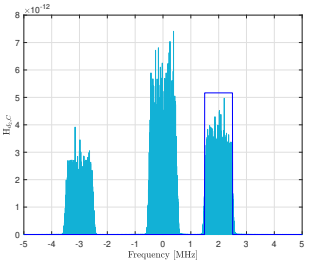

(c) $H_{2,C}$

Figure 6: Filters antenna **2**

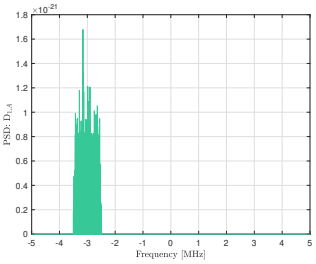

(a) PSD: $D_{1,A}$

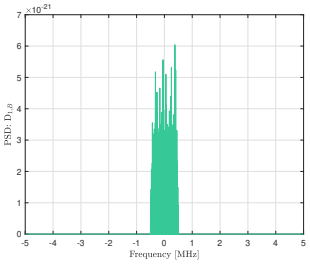

(b) PSD: $D_{1,B}$

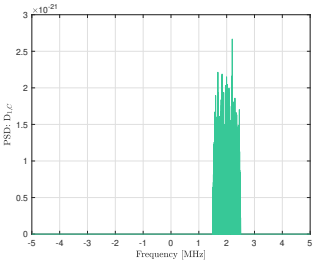

(c) PSD: $D_{1,C}$

Figure 7: Power spectra received by antenna **1**

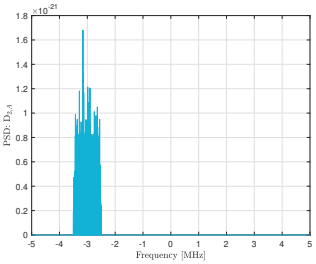

(a) PSD: $D_{2,A}$

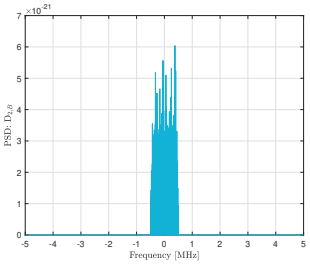

(b) PSD: $D_{2,B}$

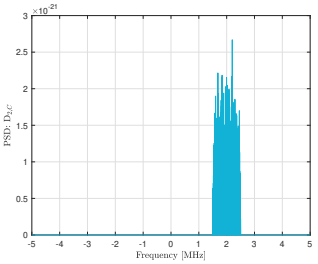

(c) PSD: $D_{2,C}$

Figure 8: Power spectra received by antenna **2**

2.5 Estimate the equivalent brightness temperature of each detected source and assess the theoretical accuracy of the estimation

In order to estimate the equivalent brightness temperatures Eq. 1 and Eq. 2 are exploited once again. Here, however, the bandwidths are different for each case, depending on the antenna considered and also on the emitting source. The results are tabulated in Tab. 10:

Table 10: Powers and brightness temperatures for each case

Source	Antenna	**Power**	**Temperature**	σ_T
A	**1**	$1.370454 \cdot 10^{-16}$ W	9.8802 K	0.0986 K
B	**1**	$5.482538 \cdot 10^{-16}$ W	39.6459 K	0.3961 K
C	**1**	$2.694134 \cdot 10^{-16}$ W	19.4171 K	0.1937 K
A	**2**	$1.370452 \cdot 10^{-16}$ W	9.8801 K	0.0986 K
B	**2**	$5.482518 \cdot 10^{-16}$ W	39.6455 K	0.3961 K
C	**2**	$2.694137 \cdot 10^{-16}$ W	19.4169 K	0.1937 K

The brightness temperatures of Tab. 10 are different from the ones obtained in section 2.1. However, the total powers are the same: if the three contributions for each antenna are summed, the same values of Tab 4 are obtained, in fact:

$$P_i = \sum_{j=1}^{3} P_{i,j} \tag{12}$$

where i = 1, 2 are the antennas and j = 1 (A), 2 (B), 3 (C) the three sources.

Table 11: Total powers for each antenna

Antenna	Total power
1	$9.547126 \cdot 10^{-16}$ W
2	$9.547106 \cdot 10^{-16}$ W

The power results obtained for each antenna for the same source are slightly different from each other, but since the errors are of the order of 10^{-20}~ 10^{-21} they could be due to the filters or related to computational errors.

2.6 Propose and implement an algorithm to estimate the direction of arrival of the radiated signals

In order to determine the directions of the signals emitted by the sources, their own phases and phase differences detected by the antennas have been considered.
Indeed, when each signal reaches the two antennas the resultant vectors are saved differently; hence, the phase of the two received signals are different as well. So in order to understand the direction of arrival and to identify the angle of every source, the phase difference between each couple of vectors that correspond to the very same source is exploited.

The wave length of the signals is expressed in Eq. 13:

$$\lambda = \frac{c}{f_0} \tag{13}$$

Eq. 14 evaluates for each emitting source the angle $\Delta\varphi$ between the signals perceived by the two antennas; the values are obtained using their product (since they are complex signals the conjugate is used as well) and then taking the mean value of it, since the result is a vector.
Then Eq. 15 [1] has been applied in order to compute the direction of arrival from each detected source.

$$\begin{cases} \Delta\varphi_j = \text{MEAN}[\angle(d_{1,j} d_{2,j}^*)] & (14) \\ \psi_j = \arcsin(\lambda \dfrac{\Delta\varphi_j}{2\pi\Delta x}) & (15) \end{cases}$$

where 1, 2 are the antennas and j = 1 (A), 2 (B), 3 (C) the three sources.
The results are reported in Tab. 12:

Table 12: Phase differences ($\Delta\varphi$) and direction of arrival (ψ) of the signals

Source	$\Delta\varphi$ [°]	ψ [°]
A	$-6.09411 \cdot 10^{-5}$	$-4.09820 \cdot 10^{-8}$
B	-148.80577	-0.10007
C	74.40498	0.05004

2.7 Evaluate empirically the accuracy of the estimation of the angle of arrival at point 6

In order to evaluate empirically the accuracy of the estimation of the angles of arrival the standard deviation of the phase differences ($\sigma_{\Delta\varphi}$) have been computed, since it is a measure of the interval of confidence.

Table 13: Accuracy of the angles

Source	$\sigma_{\Delta\varphi}$ [°]
A	0.818659
B	0.143582
C	0.996501

3 Problem 2: Estimation in SAR Interferometry

3.1 Propose an algorithm to estimate terrain topography and the displacement rate (z, v) at any pixel location from the set of interferometric phases φ(x, y, n)

In order to estimate the terrain topography and displacement rate the Best Linear Unbiased Estimator (BLUE) has been exploited, in order to obtain the minimum variance.
The collection of samples have been repeated 6 times, number given by the size of the third component of φ. The chosen algorithm that analyses the problem hence consists in a double loop, one related to the x component, the other for y (see Tab. 14).

Table 14: Number of samples

Name	**Value**
N_y	233
N_x	427

Thus, for each value of x and y the following steps have been carried out:

1. the values of φ for this particular couple (x, y) are saved in a column vector y (6x1);
2. matrix A is evaluated:
$$A = [k_z; k_v] \tag{16}$$
where, since k_z and k_v are column vectors (6x1), A is a (6x2) matrix, which columns have the values one of z and the other of v that correspond to the six different evaluations for each pixel;
3. matrix B is evaluated as well, as follows in Eq. 17:
$$\begin{cases} B^T = (A^T C_w^{-1} A)^{-1} A^T C_w^{-1} & (17) \\ B^T A = \mathcal{I} & (18) \end{cases}$$
where B is still a (6x2) matrix and C_w a (6x6). Indeed, this last matrix represents the noise covariance and is directly proportional to the standard variation of it (σ_w) as shown in Eq. 19:
$$C_w = \sigma_w^2 \mathcal{I} \tag{19}$$

where $\mathcal{I}$ is the 6x6 identity matrix. In this case, since the matrix C_w is proportional to the identity matrix, then the results of the BLUE estimation are equal to the ones that would have been obtained with the Least Squares method;

4. once B is evaluated then the estimations of z and v are known as well, since as reported in Eq. 20 the column vector $\underline{x}$ that contains their values is obtained multiplying the transpose of matrix B to y:

$$\begin{cases} \underline{x} = B^T y & (20) \\ \underline{x} = [z, v]^T & (21) \end{cases}$$

3.2 Evaluate estimation accuracy on a theoretical basis

The theoretical accuracy can be evaluated through the matrices computed before. Indeed, the covariance matrix of the estimator is:

$$C_{\hat{x}} = \begin{bmatrix} {\sigma_{\hat{x_1}}}^2 & \text{COV}(\hat{x_1}, \hat{x_2}) \\ \text{COV}(\hat{x_1}, \hat{x_2}) & {\sigma_{\hat{x_2}}}^2 \end{bmatrix} \quad (22)$$

where in the diagonal there are the values of the variances (or the square of standard deviations). Hence, applying Eq. 22 the following results are obtained:

Table 15: Standard deviations of the estimations

σ	**Value**
$\sigma_{\hat{z}}$	7.201651 m
$\sigma_{\hat{v}}$	0.258226 $\frac{m}{s}$

3.3 Apply the estimation algorithm on the data-set, and assess estimation accuracy empirically based on the knowledge of true topography and displacement rate

Through the application of the method described in section 3.1 the plots of Fig. 9b and Fig. 10b are obtained; they represent the estimation of the topography and the displacement rate for each pixel.

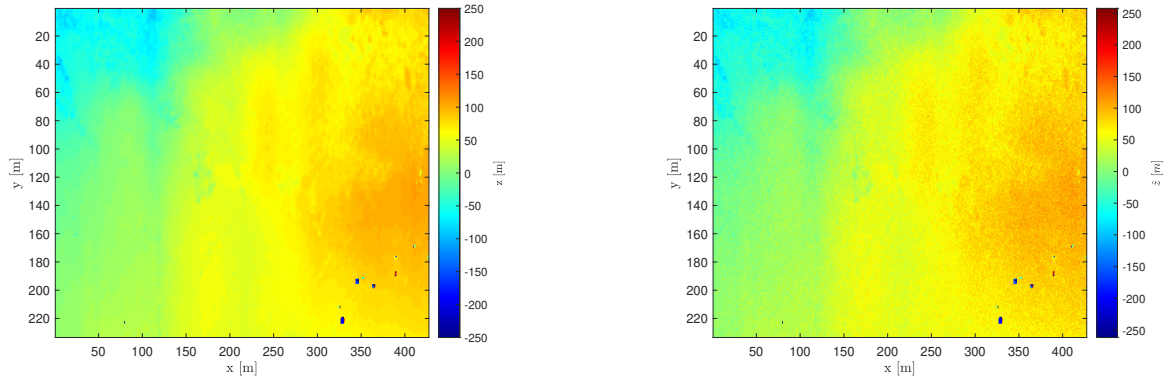

(a) True: z **(b)** Estimation: $\hat{z}$

Figure 9: Topography $[m]$

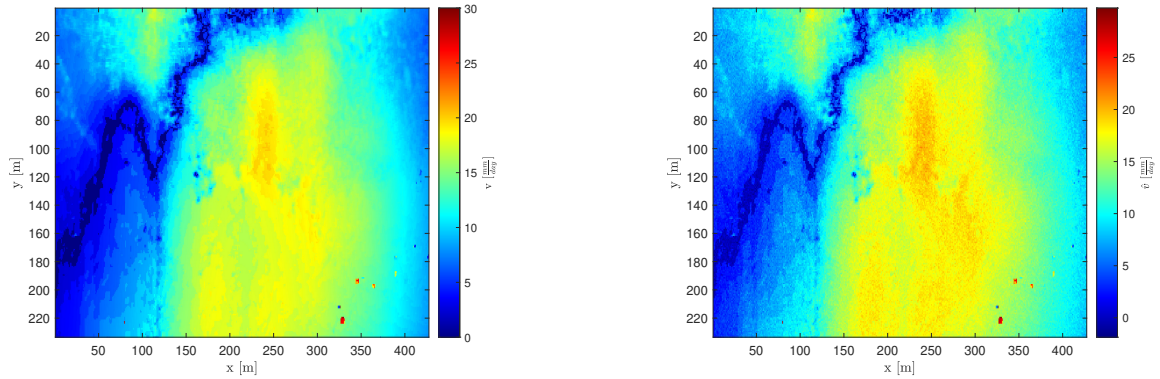

(a) True: v **(b)** Estimation: $\hat{v}$

Figure 10: Displacement rate $[\frac{mm}{day}]$

In order to assess the accuracy of the estimation, the errors have been evaluated for z and v, as the differences between the true data and the estimated ones. Then their standard deviations have been calculated, which results are shown in Tab. 17.
The theoretical standard deviations (Tab. 15) are higher than the ones just evaluated. This difference can be due to the error in the estimation and to the phase difference related to each measure.

Table 16: Standard deviations of the estimations

σ	**Value**
σ_z	7.369672 m
σ_v	0.548027 $\frac{mm}{day}$

3.4 Discuss whether estimation accuracy can be further reduced by spatial filtering, and to what extent

Spatial filtering can lead to a reduction of the accuracy of detection, by preserving the phase patterns and keeping more texture details while reducing the noise.
For this purpose, a 6-th order (due to the six collections) low-pass filter has been used, built with MATLAB function FIR1. Then the matrices have been filtered firstly row-wise, then column-wise, with a cut-off frequency of 0.52. This value has been achieved varying it between 0 and 1 and selecting the one that led to the minimum standard deviations between the true value and the result.
To obtain the results shown in Fig. 11a and Fig. 11b the same procedure described in the previous sections has been applied.

Table 17: Standard deviations after the filtering

σ	**Value**
σ_z	4.724589 m
σ_v	0.475060 $\frac{mm}{day}$

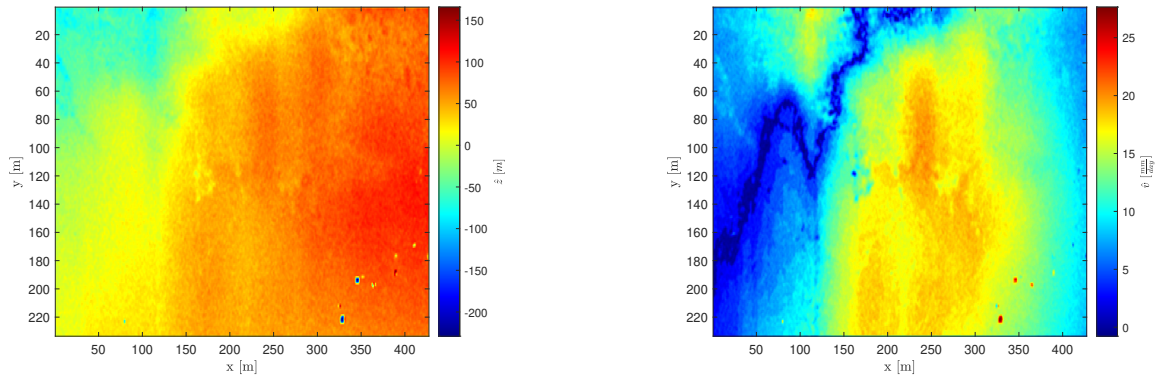

(a) Topography **(b)** Displacement rate

Figure 11: Filtered topography and displacement rate

Even though the filter is applied to smooth the images and to reduce the "noises", Fig. 11a and Fig. 11b still contain some spots but however they reproduce better results than Fig. 9b and Fig. 10b. In any case, the accuracy can be reduced and the image can be smoother, achieving a lower standard deviation.

3.5 Assume that the $\mathbf{k}_z$ (n) and $\mathbf{k}_v$ (n) conversion factors are proportional to each other, i.e.: $\mathbf{k}_z$ (n) $= \alpha\ \mathbf{k}_v$ (n), where α is some constant. What would be the impact on estimation accuracy on topography and displacement rate?

When k_z and k_v are directly proportional, the matrix of Eq. 16 is formed by two linearly dependent column vectors, since they are parallel.
Hence during the evaluation of the matrix of Eq. 17, the calculation itself cannot be performed, since the following resultant matrix is singular and then cannot be inverted:

$$A^T C_w^{-1} A$$

So since this matrix becomes singular as the topography and displacement rate are proportional, then it becomes impossible to distinguish between them and their estimation cannot be performed.

References

[1] Hongwei Zhao, Zichun Zhang, Xiaozhu Shi, Haowei Xu *A High Precision Direction-Finding Method Based on Multi-Baseline for Target Rescue*. Springer Science+Business Media, LLC, part of Springer Nature 2020. 1 June 2020
`https://doi.org/10.1007/s11036-020-01562-y`